

Structural dissection of hadronic molecules: The $D^{(*)}\bar{K}^{(*)}$ family under QCD light-cone sum rules

Ulaş Özdem¹, *

¹Health Services Vocational School of Higher Education,
Istanbul Aydin University, Sefakoy-Kucukcemece, 34295 Istanbul, Türkiye

We investigate the static electromagnetic properties of three charm–strange molecular tetraquark candidates with quantum numbers $J^P = 1^+$, namely the $D\bar{K}^*$, $D^*\bar{K}$, and $D^*\bar{K}^*$ systems. The analysis is carried out within the framework of QCD light-cone sum rules, using interpolating currents constructed from colour-singlet meson bilinears to reflect their molecular configurations. Both perturbative and non-perturbative photon contributions are included, and numerical predictions for the magnetic and electric quadrupole moments are obtained. The magnetic moments are found to lie in the range 1–3 nuclear magnetons, with the largest value associated with the $D^*\bar{K}$ configuration. The quadrupole moments are an order of magnitude smaller, of order 10^{-3} fm², indicating only weak deviations from spherical charge distributions. A flavour decomposition shows that the magnetic response is dominated by the light quarks, while the charm-quark contribution is strongly suppressed, a feature naturally expected for loosely bound hadronic molecules. The present analysis extends QCD light-cone sum-rule studies of exotic hadrons by providing a systematic determination of the electromagnetic moments of the $D^{(*)}\bar{K}^{(*)}$ molecular systems. These results provide quantitative benchmarks that may help discriminate between molecular configurations and more compact multiquark interpretations and may offer useful guidance for future experimental studies of electromagnetic signatures of charm–strange exotic states.

I. INTRODUCTION AND MOTIVATION

The discovery of exotic hadrons—states whose quark content defies the traditional meson ($q\bar{q}$) and baryon (qqq) classifications—has revolutionized our understanding of quantum chromodynamics (QCD). The journey began with the observation of the $X(3872)$ by Belle in 2003 [1], which was quickly confirmed by several experiments and could not be accommodated within the charmonium spectrum. Since then, a wealth of unconventional resonances, collectively labeled as XYZ states, pentaquarks, and tetraquarks, has been reported at facilities worldwide, including LHCb, Belle, BESIII, CMS, and others. These discoveries have sparked intense theoretical activity, as standard quark-model pictures are inadequate to describe their properties. Comprehensive reviews document the experimental progress and the diverse theoretical interpretations put forward to explain them [2–17].

A particularly active frontier is the charm–strange sector, where LHCb has recently reported several tetraquark candidates. In analyses of $B^+ \rightarrow D^+ D^- K^+$ decays, two resonances— $T_{cs0}(2900)^0$ and $T_{cs1}(2900)^0$ —were observed with minimal quark content $\bar{c}s\bar{u}\bar{d}$ [18, 19]. Their quantum numbers were determined to be $J^P = 0^+$ and $J^P = 1^-$, respectively. Subsequently, in studies of B decays to $D_s\pi$ final states, LHCb identified two additional states, $T_{a\,cs}(2900)^0$ and $T_{a\,cs}(2900)^{++}$, forming an isospin triplet with $I(J^P) = 1(0)^+$ [20, 21]. In 2024, the LHCb Collaboration carried out an analysis of resonant structures in the decays $B^+ \rightarrow D^{*+} D^- K^+$ and $B^+ \rightarrow D^{*-} D^+ K^+$, using proton–proton collision data collected at centre-of-mass energies of $\sqrt{s} = 7, 8$, and 13 TeV [22]. In addition to several charmonium-like states, including $\eta_c(3945)$, $h_c(4000)$, $\chi_{c1}(4010)$, and $h_c(4300)$, the analysis confirmed the presence of the $T_{\bar{c}s0}^*(2870)^0$ and $T_{\bar{c}s1}^*(2900)^0$ resonances in the $D^- K^+$ invariant mass spectrum. These structures, previously observed in the $B^+ \rightarrow \bar{D}^+ D^- K^+$ decay channel, were thus established in an independent production mode, with measured masses and decay widths consistent with earlier observations. All these resonances lie near 2.9 GeV, firmly establishing the existence of four-quark systems containing both charm and strange quarks. While the experimentally established states carry $J^P = 0^+$ or 1^- , theoretical models predict that the same quark constituents should also form resonances with other quantum numbers, notably $J^P = 1^+$ and 2^+ [23–27]. To elucidate the internal structure of these systems—whether they are compact tetraquarks, loosely bound meson-molecule combinations, or other configurations—it is essential to study observables beyond masses and decay widths. Electromagnetic moments offer precisely such a probe: the magnetic dipole moment reflects the distribution of circulating currents, while the electric quadrupole moment measures the deviation from a spherical charge distribution. These moments are sensitive to the spatial wave function and spin alignment of the constituents, providing distinctive fingerprints that can discriminate among different structural models.

* ulasozdem@aydin.edu.tr

In this work we compute the magnetic and quadrupole moments of three $J^P = 1^+$ molecular candidates: $D\bar{K}^*$, $D^*\bar{K}$, and $D^*\bar{K}^*$. The calculation is performed within the framework of light-cone sum rules (LCSR) [28–30], a method that combines QCD operator-product expansion near the light cone with dispersion relations. The LCSR approach systematically incorporates both short-distance (perturbative) photon couplings and long-distance effects described by photon distribution amplitudes. It has been successfully applied to electromagnetic properties of conventional and singly-heavy hadrons [26, 31–40], and here we extend it to charm-strange tetraquark systems. Our results provide quantitative predictions for electromagnetic moments that can be confronted with future experimental data, for instance from photon-induced production or from angular analyses of radiative decays. Moreover, the pattern of moments—especially the relative sizes of light-quark and charm-quark contributions—offers clues about the molecular or compact nature of the states. The present study thus complements earlier spectroscopic investigations and adds a new dimension to the characterization of exotic charm-strange hadrons.

The paper is organized as follows. In Sec. II we introduce the LCSR formalism, construct the correlation functions appropriate for each molecular configuration, and derive the sum rules for the magnetic and quadrupole moments. Section III contains the numerical analysis: we specify the input parameters, determine the working windows of the sum-rule auxiliary parameters, and present the resulting moments together with an error estimate. Finally, Sec. IV summarizes our findings and discusses their implications for future experimental searches and for the broader understanding of exotic hadron structure. Lengthy expressions for the spectral densities are relegated to the Appendix.

II. THEORETICAL FRAMEWORK FOR ELECTROMAGNETIC PROPERTIES

A. Correlation function and external field formulation

The electromagnetic properties of the charm-strange molecular tetraquark states (for short T_{cs})—specifically their magnetic (μ) and quadrupole (\mathcal{D}) moments—can be systematically extracted using light-cone sum rules (LCSR). The analysis begins with the three-point correlation function

$$T_{\mu\nu\alpha}(p, q) = i^2 \int d^4x \int d^4y e^{ip\cdot x + iq\cdot y} \langle 0 | \mathcal{T}\{J_\mu(x) J_\alpha^{em}(y) J_\nu^\dagger(0)\} | 0 \rangle, \quad (1)$$

where $J_\alpha^{em} = \sum_q e_q \bar{q} \gamma_\alpha q$ is the electromagnetic current (e_q being the quark electric charge), and $J_\mu(x)$ denotes an interpolating current that couples to the $J^P = 1^+$ tetraquark state. The correlator in Eq. (1) probes the matrix element $\langle T_{cs}(p) | J_\alpha^{em} | T_{cs}(p') \rangle$ through analytic continuation, where the initial and final tetraquark momenta are p and $p' = p + q$, respectively.

In practice, it is technically advantageous to reformulate the problem using an external background electromagnetic field. Replacing the explicit photon insertion by a classical, slowly varying field $A_\mu^{\text{ext}}(x)$, one considers instead the two-point function

$$T_{\mu\nu}(p, q) = i \int d^4x e^{ip\cdot x} \langle 0 | \mathcal{T}\{J_\mu(x) J_\nu^\dagger(0)\} | 0 \rangle_F, \quad (2)$$

where the subscript F indicates that the vacuum expectation value is evaluated in the presence of the external field. The field strength tensor is taken in momentum space as

$$F_{\alpha\beta} = i(\varepsilon_\alpha q_\beta - \varepsilon_\beta q_\alpha) e^{-iq\cdot x},$$

with q and ε being the four-momentum and polarization vector of the background photon.

Advantages of the external-field method: (i) Gauge invariance is maintained manifestly; (ii) soft (non-perturbative) and hard (perturbative) photon emissions are separated cleanly; (iii) the photon light-cone distribution amplitudes (LCDAs) enter naturally, organizing the operator product expansion (OPE) in powers of the photon virtuality [41].

Because the external field is weak, the correlation function can be expanded as

$$T_{\mu\nu}(p, q) = T_{\mu\nu}^{(0)}(p) + T_{\mu\nu}^{(1)}(p, q) + \mathcal{O}(F^2), \quad (3)$$

where $T_{\mu\nu}^{(0)}$ corresponds to the free propagation of the tetraquark (giving rise to mass sum rules) and $T_{\mu\nu}^{(1)}$ is linear in the field strength. Only the latter term contains the information on electromagnetic multipole moments [41–43].

The formulation outlined above allows us to compute the electromagnetic moments of the tetraquark states within the LCSR approach. The actual calculation proceeds in three consecutive steps:

- Hadronic representation: Using dispersion relations, the correlation function is expressed in terms of the tetraquark's mass m , coupling λ (defined by $\langle 0|J_\mu|T_{cs}\rangle = \lambda \varepsilon_\mu$), and electromagnetic form factors. The contribution of the ground state is isolated, while higher resonances and the continuum are parametrized through a spectral density.
- QCD representation: The same correlation function is computed via the OPE near the light cone ($x^2 \sim 0$). The short-distance part is treated perturbatively, while the long-distance interaction of the photon with the QCD vacuum is encoded in photon LCDAs of increasing twist. This yields $T_{\mu\nu}^{\text{QCD}}$, written explicitly in terms of quark-gluon degrees of freedom.
- Matching and Borel transformation: The two representations are matched assuming quark-hadron duality. To suppress contributions from excited states and enhance the ground-state pole, a double Borel transformation with respect to $-p^2$ and $-p'^2$ is applied. After subtracting the continuum using a suitable threshold s_0 , one obtains sum rules for the magnetic and quadrupole moments.

In the following sections, we first specify the interpolating currents for the T_{cs} molecular states, then derive the hadronic and QCD sides in detail, and finally extract the sum rules for the electromagnetic moments.

B. Interpolating currents for the T_{cs} molecular states

The construction of appropriate interpolating currents is a key step in the QCD sum-rule analysis of multiquark states, since the chosen operators determine which hadronic configurations are preferentially selected from the QCD vacuum. For the molecular-type T_{cs} tetraquarks studied here, we employ currents that are explicitly built from colour-singlet meson bilinears. This reflects the underlying physical picture: the states are assumed to be dominantly composed of two weakly bound, colourless mesons. Such a construction emphasises the long-distance, molecular component of the wave function, in contrast to compact diquark–antidiquark currents, which would probe a more spatially concentrated configuration. The interpolating currents for the three T_{cs} molecular systems are defined as

$$J_\mu^1(x) = [\bar{q}_a(x)\gamma_5 c_a(x)] [\bar{q}_b(x)\gamma^\mu s_b(x)], \quad (4)$$

$$J_\mu^2(x) = [\bar{q}_a(x)\gamma^\mu c_a(x)] [\bar{q}_b(x)\gamma_5 s_b(x)], \quad (5)$$

$$J_\mu^3(x) = [\bar{q}_a(x)\gamma_\alpha c_a(x)] [\bar{q}_b(x)\sigma^{\mu\alpha}\gamma_5 s_b(x)] - [\bar{q}_a(x)\sigma^{\mu\alpha}\gamma_5 c_a(x)] [\bar{q}_b(x)\gamma_\alpha s_b(x)], \quad (6)$$

where a and b are color indices, and q denotes u or d quark fields.

The current $J_\mu^1(x)$ in Eq. (4) is constructed from the color-singlet bilinears $[\bar{q}\gamma_5 c]$ and $[\bar{q}\gamma^\mu s]$, chosen to match the quantum numbers of a $D\bar{K}^*$ system. The first bilinear represents a pseudoscalar charm meson (D), while the second corresponds to a vector strange meson (K^*). In a relative S -wave, their product yields total spin-parity $J^P = 1^+$. Therefore, J_μ^1 predominantly creates a hadronic molecular state with a $D\bar{K}^*$ configuration. Similarly, the current $J_\mu^2(x)$ in Eq. (5) is built as $[\bar{q}\gamma^\mu c] \otimes [\bar{q}\gamma_5 s]$, corresponding to a vector charm meson (D^*) and a pseudoscalar strange meson (K). Again, in an S -wave the combination gives $J^P = 1^+$, making J_μ^2 appropriate for a $D^*\bar{K}$ molecular configuration. The current $J_\mu^3(x)$ in Eq. (6) involves an antisymmetric combination of a vector bilinear and a tensor bilinear,

$$([\bar{q}\gamma_\alpha c][\bar{q}\sigma^{\mu\alpha}\gamma_5 s] - [\bar{q}\sigma^{\mu\alpha}\gamma_5 c][\bar{q}\gamma_\alpha s]), \quad (7)$$

which is designed to couple to a $D^*\bar{K}^*$ system in a spin-1 configuration. In a relative S -wave between the two vector mesons, this combination yields total spin-parity $J^P = 1^+$, providing the correct Lorentz structure for a molecular interpretation. The explicit use of color-singlet bilinears reflects the molecular picture of these states: each interpolator is constructed assuming that the physical resonance can be effectively described as a composite of two color-singlet mesons. This is in contrast to diquark–antidiquark currents of the type

$$[q^T C c][\bar{s} C \bar{q}^T], \quad (8)$$

which represents a typical compact tetraquark interpolator and is included here for illustrative purposes; such interpolators involve color-antitriplet diquarks and antidiquarks and are conceptually distinct from the color-singlet bilinear currents used for molecular states. While both molecular- and tetraquark-type currents may couple to the same physical state, the molecular currents are theoretically motivated by the proximity of the observed states to their respective meson-meson thresholds—a characteristic feature of molecular candidates. Using these interpolators, QCD sum-rule calculations can efficiently probe properties that naturally arise from a two-meson structure, including decay constants, production rates, and decay amplitudes [44].

C. QCD description of the correlation function

Within the framework of QCD, the correlation function is evaluated by inserting the interpolating currents given in Eq. (2) and performing all possible contractions using Wick's theorem. For the hadronic states under consideration, the resulting expressions for the correlation functions are

$$T_{\mu\nu}^{\text{QCD}-1}(p, q) = i \int d^4x e^{ip \cdot x} \left\langle 0 \left| \text{Tr} \left[\gamma_\mu S_s^{bb'}(x) \gamma_\nu S_q^{a'a}(-x) \right] \text{Tr} \left[\gamma_5 S_c^{aa'}(x) \gamma_5 S_q^{a'a}(-x) \right] \right| 0 \right\rangle_F, \quad (9)$$

$$T_{\mu\nu}^{\text{QCD}-2}(p, q) = i \int d^4x e^{ip \cdot x} \left\langle 0 \left| \text{Tr} \left[\gamma_5 S_s^{bb'}(x) \gamma_5 S_q^{a'a}(-x) \right] \text{Tr} \left[\gamma_\mu S_c^{aa'}(x) \gamma_\nu S_q^{a'a}(-x) \right] \right| 0 \right\rangle_F, \quad (10)$$

$$\begin{aligned} T_{\mu\nu}^{\text{QCD}-3}(p, q) = i \int d^4x e^{ip \cdot x} & \left\langle 0 \left| \text{Tr} \left[\sigma_{\mu\alpha} \gamma_5 S_s^{bb'}(x) \gamma_5 \sigma_{\nu\beta} S_q^{a'a}(-x) \right] \text{Tr} \left[\gamma_\alpha S_c^{aa'}(x) \gamma_\beta S_q^{a'a}(-x) \right] \right. \right. \\ & - \text{Tr} \left[\sigma_{\mu\alpha} \gamma_5 S_s^{bb'}(x) \gamma_\beta S_q^{a'a}(-x) \right] \text{Tr} \left[\gamma_\alpha S_c^{aa'}(x) \gamma_5 \sigma_{\nu\beta} S_q^{a'a}(-x) \right] \\ & - \text{Tr} \left[\gamma_\alpha S_s^{bb'}(x) \gamma_5 \sigma_{\nu\beta} S_q^{a'a}(-x) \right] \text{Tr} \left[\sigma_{\mu\alpha} \gamma_5 S_c^{aa'}(x) \gamma_\beta S_q^{a'a}(-x) \right] \\ & \left. \left. + \text{Tr} \left[\gamma_\alpha S_s^{bb'}(x) \gamma_\beta S_q^{a'a}(-x) \right] \text{Tr} \left[\sigma_{\mu\alpha} \gamma_5 S_c^{aa'}(x) \gamma_5 \sigma_{\nu\beta} S_q^{a'a}(-x) \right] \right| 0 \right\rangle_F, \end{aligned} \quad (11)$$

where the $T_{\mu\nu}^{\text{QCD}-1}(p, q)$, $T_{\mu\nu}^{\text{QCD}-2}(p, q)$, and $T_{\mu\nu}^{\text{QCD}-3}(p, q)$ refer to the molecular configurations $D\bar{K}^*$, $D^*\bar{K}$, and $D^*\bar{K}^*$, respectively.

The quark propagators employed in the calculation are taken in coordinate space. For a light quark ($q = u, d$ and s) the propagator reads [45]

$$S_q(x) = S_q^{\text{free}}(x) - \frac{ig_s}{16\pi^2 x^2} \int_0^1 du G^{\mu\nu}(ux) \left[\bar{u} \not{v} \sigma_{\mu\nu} + u \sigma_{\mu\nu} \not{v} \right], \quad (12)$$

and for a charm quark [46]

$$S_c(x) = S_c^{\text{free}}(x) - \frac{im_c g_s}{16\pi^2} \int_0^1 du G^{\mu\nu}(ux) \left[(\sigma_{\mu\nu} \not{v} + \not{v} \sigma_{\mu\nu}) \frac{K_1(m_c \sqrt{-x^2})}{\sqrt{-x^2}} + 2\sigma_{\mu\nu} K_0(m_c \sqrt{-x^2}) \right]. \quad (13)$$

The free (perturbative) parts are given by

$$S_q^{\text{free}}(x) = \frac{1}{2\pi^2 x^2} \left(i \frac{\not{v}}{x^2} - \frac{m_q}{2} \right), \quad (14)$$

$$S_c^{\text{free}}(x) = \frac{m_c^2}{4\pi^2} \left[\frac{K_1(m_c \sqrt{-x^2})}{\sqrt{-x^2}} + i \frac{\not{v} K_2(m_c \sqrt{-x^2})}{(\sqrt{-x^2})^2} \right], \quad (15)$$

where $G^{\mu\nu}(x)$ is the gluon field-strength tensor and $K_n(z)$ denote modified Bessel functions of the second kind.

The photon can couple to the quark lines either perturbatively, through the elementary QED vertex, or non-perturbatively, via the photon distribution amplitudes (DAs). A consistent treatment requires the inclusion of both mechanisms. Their implementation proceeds as follows:

- Perturbative (short-distance) photon emission: The photon couples directly to a quark line via the substitution

$$S_{c(q)}^{\text{free}}(x) \longrightarrow \int d^4z S_{c(q)}^{\text{free}}(x-z) A(z) S_{c(q)}^{\text{free}}(z), \quad (16)$$

where $A_\mu(z)$ is the photon field. This replacement is applied to one quark propagator (light or heavy) while the remaining propagators are kept in their free form.

- Non-perturbative (long-distance) photon emission: The photon couples to the QCD vacuum through light-quark condensates and photon DAs. This effect is incorporated by replacing one light-quark propagator according to [46]

$$S_{q,\alpha\beta}^{ab}(x) \longrightarrow -\frac{1}{4} [\bar{q}^a(x) \Gamma_i q^b(0)] (\Gamma_i)_{\alpha\beta}, \quad (17)$$

with $\Gamma_i = \{\mathbb{1}, \gamma_5, \gamma_\mu, i\gamma_5\gamma_\mu, \sigma_{\mu\nu}/2\}$. The resulting matrix elements of the form $\langle \gamma(q)|\bar{q}(x)\Gamma_i q(0)|0\rangle$ and $\langle \gamma(q)|\bar{q}(x)\Gamma_i G_{\alpha\beta}q(0)|0\rangle$ are expressed in terms of photon DAs of increasing twist [41]. In this work, the long-distance (non-perturbative) photon couplings are included only via photon distribution amplitudes involving light quarks (u, d, s). Contributions from heavy-quark (charm) photon DAs are omitted because they are suppressed by powers of the heavy-quark mass $1/m_c$ —a well-established feature in QCD sum rule and effective field theory treatments of heavy hadrons [47]. This suppression reflects the fact that the polarization of the QCD vacuum due to heavy quarks is parametrically smaller than that due to light quarks. Consequently, heavy quarks contribute only through perturbative photon emission, while the non-perturbative photon structure is captured entirely by light-quark degrees of freedom.

The systematic combination of the perturbative and non-perturbative photon couplings leads to the complete QCD representation of the correlation function. The explicit evaluation of the resulting integrals, together with a subsequent matching to the hadronic representation, will allow the extraction of the electromagnetic properties of the states under study.

D. Hadronic description of the correlation function

The hadronic representation of the correlation function is obtained by saturating it with a complete set of hadronic states possessing the same quantum numbers as the interpolating currents. After inserting these intermediate states and isolating the contribution of the lowest-lying T_{cs} tetraquark state, the correlation function can be written as

$$T_{\mu\nu}^{\text{Had}}(p, q) = \frac{1}{[p^2 - m_{T_{cs}}^2][p'^2 - m_{T_{cs}}^2]} \langle 0|J_\mu(x)|T_{cs}(p, \varepsilon^i)\rangle \langle T_{cs}(p, \varepsilon^i)|T_{cs}(p', \varepsilon^f)\rangle_F \langle T_{cs}(p', \varepsilon^f)|J_\nu^\dagger(0)|0\rangle + \text{higher resonances and continuum contributions.} \quad (18)$$

To proceed, the explicit forms of the matrix elements appearing in the above expression are required. The overlap between the tetraquark state and the interpolating current is parametrized by

$$\langle 0|J_\mu(x)|T_{cs}(p, \varepsilon^i)\rangle = \lambda_{T_{cs}} \varepsilon_\mu^i, \quad (19)$$

$$\langle T_{cs}(p', \varepsilon^f)|J_\nu^\dagger(0)|0\rangle = \lambda_{T_{cs}} \varepsilon_\nu^f, \quad (20)$$

where $\lambda_{T_{cs}}$ denotes the coupling of the current to the physical state, and ε_μ^i (ε_ν^f) is the polarization vector of the initial (final) tetraquark.

The matrix element describing the interaction of the tetraquark with an external photon, $\langle T_{cs}(p, \varepsilon^i)|T_{cs}(p', \varepsilon^f)\rangle_F$, can be expressed in terms of three independent Lorentz-invariant form factors $G_1(Q^2)$, $G_2(Q^2)$, and $G_3(Q^2)$ as [48]

$$\langle T_{cs}(p, \varepsilon^i)|T_{cs}(p', \varepsilon^f)\rangle_F = -\varepsilon^\gamma(\varepsilon^i)^\mu(\varepsilon^f)^\nu \left[G_1(Q^2)(p + p')_\gamma g_{\mu\nu} + G_2(Q^2)(g_{\gamma\nu} q_\mu - g_{\gamma\mu} q_\nu) - \frac{1}{2m_{T_{cs}}^2} G_3(Q^2)(p + p')_\gamma q_\mu q_\nu \right]. \quad (21)$$

Here ε^γ is the polarization vector of the photon, and $Q^2 = -q^2$ is the momentum transfer squared.

In phenomenological analyses, it is customary to employ the magnetic and quadrupole form factors, $F_M(Q^2)$ and $F_D(Q^2)$, which are linear combinations of the $G_i(Q^2)$:

$$F_M(Q^2) = G_2(Q^2),$$

$$F_D(Q^2) = G_1(Q^2) - G_2(Q^2) + \left(1 + \frac{Q^2}{4m_{T_{cs}}^2}\right) G_3(Q^2). \quad (22)$$

For real-photon processes ($Q^2 = 0$), these form factors reduce to the static electromagnetic moments of the tetraquark:

$$\mu_{T_{cs}} = \frac{e}{2m_{T_{cs}}} F_M(0), \quad (23)$$

$$\mathcal{D}_{T_{cs}} = \frac{e}{m_{T_{cs}}^2} F_D(0). \quad (24)$$

Substituting Eqs. (19)–(22) into Eq. (18) and expressing the result in terms of $F_M(0)$ and $F_D(0)$ yields the hadronic representation of the correlation function relevant for the static limit:

$$T_{\mu\nu}^{\text{Had}}(p, q) = \frac{\lambda_{T_{cs}}^2}{[m_{T_{cs}}^2 - p^2][m_{T_{cs}}^2 - p'^2]} \left[F_M(0) \left(q_\mu \varepsilon_\nu - q_\nu \varepsilon_\mu + \frac{(\varepsilon \cdot p)}{m_{T_{cs}}^2} (p_\mu q_\nu - p_\nu q_\mu) \right) - F_D(0) \frac{(\varepsilon \cdot p)}{m_{T_{cs}}^2} q_\mu q_\nu \right]. \quad (25)$$

The above expression provides the starting point for extracting the magnetic and quadrupole moments of the T_{cs} tetraquark, thereby completing the hadronic side of the analysis.

E. LCSR for the electromagnetic moments

The extraction of the electromagnetic moments proceeds through a systematic analysis of the correlation function within the LCSR framework. The key step involves matching the hadronic and QCD representations of the correlation function. Specifically, the magnetic moment is obtained by isolating the coefficient of the antisymmetric tensor structure ($\varepsilon_\mu q_\nu - \varepsilon_\nu q_\mu$), which is unique to the magnetic dipole interaction in the static limit ($Q^2 = 0$). After performing the double Borel transformation with respect to the variables $-p^2$ and $-p'^2$ to suppress continuum contributions, we arrive at the master sum rule

$$\mu_{T_{cs}} \lambda_{T_{cs}}^2 e^{-m_{T_{cs}}^2/M_1^2} e^{-m_{T_{cs}}^2/M_2^2} = T_{\mu\nu}^{\text{QCD}}(M_1^2, M_2^2), \quad (26)$$

where $T_{\mu\nu}^{\text{QCD}}(M_1^2, M_2^2)$ denotes the Borel-transformed OPE expression.

To account for the continuum and excited states, the quark–hadron duality is employed. In the double dispersion relation, the physical spectral density is approximated by its OPE counterpart above a duality threshold s_0 . For the diagonal correlation function considered here, a natural choice is the triangular duality region

$$\frac{s_1}{M_1^2} + \frac{s_2}{M_2^2} < \frac{s_0}{M^2}, \quad (27)$$

with the effective Borel mass defined as $M^2 = M_1^2 M_2^2 / (M_1^2 + M_2^2)$. Introducing the variables

$$s = \frac{M_1^2 s_2 + M_2^2 s_1}{M_1^2 + M_2^2}, \quad u = \frac{M_2^2 s_1}{M_1^2 s_2 + M_2^2 s_1}, \quad (28)$$

the double integral can be reduced to a single one:

$$T_{\mu\nu}^{\text{QCD}}(M_1^2, M_2^2) = \int_0^{s_0} ds e^{-s/M^2} \tilde{\rho}(s), \quad (29)$$

where the transformed spectral density $\tilde{\rho}(s)$ incorporates an integral over the mixing parameter u .

For elastic scattering, the initial and final tetraquark masses are equal, which allows us to symmetrize the Borel parameters by setting $M_1^2 = M_2^2 = 2M^2$. This simplifies the expressions considerably and leads to the final LCSR formulas for the magnetic and quadrupole moments of the three molecular configurations:

$$\mu_{D\bar{K}^*} = \frac{e^{m_{D\bar{K}^*}^2/M^2}}{\lambda_{D\bar{K}^*}^2} \mathcal{R}_1(M^2, s_0), \quad \mathcal{D}_{D\bar{K}^*} = \frac{e^{m_{D\bar{K}^*}^2/M^2}}{\lambda_{D\bar{K}^*}^2} \mathcal{R}_2(M^2, s_0), \quad (30)$$

$$\mu_{D^*\bar{K}} = \frac{e^{m_{D^*\bar{K}}^2/M^2}}{\lambda_{D^*\bar{K}}^2} \mathcal{R}_3(M^2, s_0), \quad \mathcal{D}_{D^*\bar{K}} = \frac{e^{m_{D^*\bar{K}}^2/M^2}}{\lambda_{D^*\bar{K}}^2} \mathcal{R}_4(M^2, s_0), \quad (31)$$

$$\mu_{D^*\bar{K}^*} = \frac{e^{m_{D^*\bar{K}^*}^2/M^2}}{\lambda_{D^*\bar{K}^*}^2} \mathcal{R}_5(M^2, s_0), \quad \mathcal{D}_{D^*\bar{K}^*} = \frac{e^{m_{D^*\bar{K}^*}^2/M^2}}{\lambda_{D^*\bar{K}^*}^2} \mathcal{R}_6(M^2, s_0). \quad (32)$$

The functions $\mathcal{R}_i(M^2, s_0)$ ($i = 1, \dots, 6$) represent the QCD spectral integrals for each state and moment. The spectral functions $\mathcal{R}_1(M^2, s_0)$, $\mathcal{R}_3(M^2, s_0)$, and $\mathcal{R}_5(M^2, s_0)$ on the right-hand side correspond to the magnetic moments of the $D\bar{K}^*$, $D^*\bar{K}$, and $D^*\bar{K}^*$ states, respectively. Their explicit forms, which follow from a lengthy evaluation of the QCD side including both perturbative and non-perturbative photon couplings, are provided in the Appendix for completeness.

III. NUMERICAL ASPECTS

A. Input parameters

The numerical evaluation of the magnetic and quadrupole moments within the LCSR framework requires the specification of various input parameters, which are collected in Table I. The photon DAs encode the nonperturbative interaction of the photon with the QCD vacuum and are essential ingredients of the external-field LCSR. Their explicit forms, which involve the parameter $f_{3\gamma}$ listed in the table, are taken from Ref. [41].

TABLE I. Summary of input parameters used in the LCSR analysis. The references are: (a) [49]; (b) [50, 51]; (c) [44]; (d) [52]; (e) [41].

Parameter	Value	Ref.
Quark masses		
$m_u = m_d$	0	-
m_s	93.5 ± 0.08 MeV	(a)
m_c	1.273 ± 0.0046 GeV	(a)
Vacuum condensates		
$\langle \bar{u}u \rangle = \langle \bar{d}d \rangle$	$(-0.24 \pm 0.01)^3$ GeV ³	(b)
$\langle \bar{s}s \rangle$	$(0.8 \pm 0.1) \langle \bar{u}u \rangle$	(b)
$\langle g_s^2 G^2 \rangle$	0.48 ± 0.14 GeV ⁴	(b)
Tetraquark parameters		
$m_{D\bar{K}^*}$	$2.89^{+0.10}_{-0.11}$ GeV	(c)
$\lambda_{D\bar{K}^*}$	$(8.6^{+0.19}_{-0.17}) \times 10^{-2}$ GeV ⁵	(c)
$m_{D^*\bar{K}}$	$2.85^{+0.10}_{-0.11}$ GeV	(c)
$\lambda_{D^*\bar{K}}$	$(0.82^{+0.18}_{-0.17}) \times 10^{-2}$ GeV ⁵	(c)
$m_{D^*\bar{K}^*}$	$3.13^{+0.12}_{-0.13}$ GeV	(c)
$\lambda_{D^*\bar{K}^*}$	$(2.96^{+0.62}_{-0.55}) \times 10^{-2}$ GeV ⁵	(c)
Photon DAs parameters		
χ	-2.85 ± 0.5 GeV ⁻²	(d)
$f_{3\gamma}$	-0.0039 GeV ²	(e)

B. Stability and reliability of LCSR

According to Eqs. (30)–(32), the LCSR predictions depend on two auxiliary parameters: the continuum threshold s_0 and the Borel mass parameter M^2 . Although these parameters are not physical observables, the extraction of reliable magnetic and quadrupole moments requires identifying regions in which the results exhibit minimal sensitivity to their variation. These regions define the working windows of the sum rules. The continuum threshold s_0 accounts for the onset of excited states and continuum contributions in the hadronic representation of the correlation function. Phenomenologically, it is expected to lie slightly above the squared mass of the ground state. Guided by standard QCD sum-rule practice, we adopt the interval $(m_H + 0.5)^2$ GeV² $\leq s_0 \leq (m_H + 0.7)^2$ GeV², where m_H denotes the mass of the hadronic state under consideration. This choice is known to provide stable predictions in closely related analyses and is used throughout this work. The Borel window for M^2 is determined by two competing constraints. The lower bound is fixed by the convergence of the OPE, requiring that higher-dimensional condensate contributions remain suppressed. The upper bound is constrained by pole dominance, ensuring that the ground-state contribution is not overwhelmed by the continuum. These requirements are quantified through the conditions

$$\text{PC} = \frac{\mathcal{R}_i(M^2, s_0)}{\mathcal{R}_i(M^2, \infty)} > 40\%, \quad (33)$$

$$\text{CVG} = \frac{\mathcal{R}_i^{\text{Dim 7}}(M^2, s_0)}{\mathcal{R}_i(M^2, s_0)} < 5\%, \quad (34)$$

where $\mathcal{R}_i^{\text{Dim 7}}(M^2, s_0)$ denotes the highest-dimensional term retained in the OPE for the invariant function $\mathcal{R}_i(M^2, s_0)$.

Imposing these criteria simultaneously, we determine the working regions for M^2 and s_0 , summarized in Table II. Within these windows, the PC amounts to 40–70% for all channels, confirming the dominance of the lowest-lying state and justifying the single-pole approximation adopted in the hadronic parametrization. At the same time, the OPE exhibits excellent convergence: the relative contribution of the dimension-7 terms remains below 0.5% over the entire Borel window, indicating that the convergence condition is satisfied with a large safety margin well within the adopted 5% criterion. The reliability of the sum-rule extraction requires the simultaneous satisfaction of PC and CVG, which together define the fiducial Borel working region. Within this window, the ground-state contribution must

TABLE II. Determination of the LCSR parameter windows in s_0 and M^2 , showing the resulting PC and CVG for the electromagnetic observables of the $D^{(*)}\bar{K}^{(*)}$ systems.

States	s_0 (GeV 2)	M^2 (GeV 2)	PC (%)	CVG (%)
$D^*\bar{K}^*$	[13.2, 14.6]	[2.0, 2.8]	[70.42, 41.41]	0.44
$D\bar{K}^*$	[11.5, 12.9]	[1.8, 2.4]	[66.55, 41.07]	0.38
$D^*\bar{K}$	[11.5, 12.9]	[2.0, 2.8]	[68.91, 40.10]	0.42

remain sizable compared to the continuum, while higher-dimensional condensate terms stay under control, ensuring the stability of the OPE. As an illustrative example, Fig. 1 displays the CVG, the PC, and the resulting magnetic moment as functions of the Borel parameter M^2 for several fixed values of s_0 in the $D^*\bar{K}^*$ channel. One observes that the PC dominates over the continuum and the OPE remains well convergent inside the adopted Borel window, while the extracted magnetic moment exhibits only a mild dependence on the auxiliary parameters M^2 and s_0 . These residual variations are incorporated into the quoted theoretical uncertainties. The fulfillment of the standard LCSR stability criteria suggests that the extracted predictions are reasonably reliable within the present analysis.

C. Numerical results

A comprehensive numerical analysis is performed to extract the magnetic and electric quadrupole moments of the $D^{(*)}\bar{K}^{(*)}$ molecular tetraquark states. The resulting central values and uncertainties are summarized in Table II. The quoted errors include the systematic propagation of all input parameters as well as the variations of the auxiliary LCSR parameters, M^2 and s_0 . The relative contributions to the total uncertainty are estimated to be approximately 15% from the tetraquark masses, 10% from quark masses, 22% from the residue parameters, 30% from the continuum threshold s_0 , 8% from the Borel mass parameter M^2 , 10% from the photon DAs, and about 5% from remaining sources such as QCD condensates. All individual uncertainties are combined in quadrature to obtain the final error bars reported in Table III.

TABLE III. Magnetic dipole and electric quadrupole moments of the $D^{(*)}\bar{K}^{(*)}$ molecular states with quark contents $[\bar{q}c][\bar{q}s]$ ($q = u, d$) obtained from LCSR.

States	μ (μ_N)	\mathcal{D} ($\times 10^{-3}$ fm 2)
$D^*\bar{K}^* - [\bar{u}c][\bar{u}s]$	1.93 ± 0.47	-0.46 ± 0.08
$D^*\bar{K}^* - [\bar{d}c][\bar{d}s]$	-0.62 ± 0.15	-0.09 ± 0.01
$D\bar{K}^* - [\bar{u}c][\bar{u}s]$	1.99 ± 0.49	3.60 ± 0.40
$D\bar{K}^* - [\bar{d}c][\bar{d}s]$	0.00 ± 0.00	0.00 ± 0.00
$D^*\bar{K} - [\bar{u}c][\bar{u}s]$	3.08 ± 0.77	6.01 ± 0.80
$D^*\bar{K} - [\bar{d}c][\bar{d}s]$	-2.04 ± 0.50	-3.01 ± 0.40

Our analysis provides quantitative information on the electromagnetic structure of the $D^{(*)}\bar{K}^{(*)}$ molecular configurations. In the following, we summarize the main features of the magnetic and quadrupole moments and discuss their physical implications.

1. Magnetic moments

The extracted magnetic moments display a clear and systematic hierarchy among the $D^{(*)}\bar{K}^{(*)}$ molecular configurations. The largest value is obtained for the charged $D^*\bar{K}$ state, $\mu = 3.08 \pm 0.77 \mu_N$, whereas the $D\bar{K}^*$ and $D^*\bar{K}^*$ channels yield smaller but comparable magnitudes of about $2 \mu_N$. This behavior can be traced to the different spin structures of the constituent mesons: the vector–pseudoscalar configuration allows a more efficient alignment of the light-quark spins with the external electromagnetic field, while in the vector–vector system partial cancellations reduce the net magnetic response. A qualitatively different pattern is observed for neutral configurations. The $D\bar{K}^*$ state exhibits a vanishing magnetic moment as a consequence of charge cancellation combined with the specific spin–flavor structure of the current, whereas the neutral $D^*\bar{K}$ and $D^*\bar{K}^*$ states remain nonzero. This indicates that these molecular combinations are not eigenstates of charge conjugation and retain nontrivial internal spin distributions capable of generating a finite magnetic moment.

The flavor decomposition (see Table IV) further demonstrates a clear dominance of the light quarks. In all channels the $u(d)$ components provide the leading contribution to the total magnetic moment. The strange-quark term remains subleading but non-negligible, typically $|\mu_s| \sim 0.4\text{--}0.7 \mu_N$, reflecting the intermediate mass of the s quark relative to the light sector. By contrast, the charm-quark contribution is strongly suppressed, $|\mu_c| \lesssim 0.3 \mu_N$, in accordance with heavy-quark symmetry, where magnetic moments scale approximately as $1/m_c$. These results establish the hierarchy

$$|\mu_{u(d)}| > |\mu_s| > |\mu_c|,$$

showing that the electromagnetic response is governed predominantly by the light constituents, while the heavy quark acts essentially as a static color source.

Consequently, at the hadronic level one obtains the ordering

$$\mu_{D^*\bar{K}} > \mu_{D\bar{K}^*} \simeq \mu_{D^*\bar{K}^*},$$

which is qualitatively consistent with expectations for a loosely bound molecular configuration, where the magnetic response is dominated by the light-quark degrees of freedom.

TABLE IV. Individual quark-flavor contributions to the magnetic moments of the $D^{(*)}\bar{K}^{(*)}$ molecular states. All quantities are expressed in units of μ_N . Here, the total magnetic moment is given by $\mu_{\text{tot}} = \mu_{u(d)} + \mu_s + \mu_c$, corresponding to the sum of the individual quark contributions.

States	μ_u	μ_d	μ_s	μ_c	μ_{tot}
$D^*\bar{K}^* - [\bar{u}c][\bar{u}s]$	1.70	–	0.44	–0.21	1.93
$D^*\bar{K}^* - [\bar{d}c][\bar{d}s]$	–	–0.85	0.44	–0.21	–0.62
$D\bar{K}^* - [\bar{u}c][\bar{u}s]$	1.33	–	0.66	0.00	1.99
$D\bar{K}^* - [\bar{d}c][\bar{d}s]$	–	0.00	0.00	0.00	0.00
$D^*\bar{K} - [\bar{u}c][\bar{u}s]$	3.41	–	0.00	–0.33	3.08
$D^*\bar{K} - [\bar{d}c][\bar{d}s]$	–	–1.71	0.00	–0.33	–2.04

2. Quadrupole moments

The electric quadrupole moments probe deviations from spherical charge distributions and therefore provide complementary information to the magnetic dipole moments about the internal spatial structure of the states. In contrast to the dipole moments, which are controlled mainly by the total spin and flavor content, the quadrupole moments are sensitive to the anisotropy of the charge distribution and require nonzero orbital or tensor components in the

wave function. Numerically, all obtained values are of order 10^{-3} fm^2 and are significantly suppressed relative to the magnetic moments. Since a quadrupole moment scales parametrically as $\mathcal{D} \sim er^2$, its small magnitude suggests only weak deviations from spherical symmetry.

Among the considered systems, the $D^*\bar{K}$ states exhibit the largest absolute magnitudes, whereas the fully neutral $D\bar{K}^*$ configuration vanishes identically due to charge symmetry. Positive values correspond to prolate shapes and negative ones to oblate deformations; accordingly, the $[\bar{u}c][\bar{u}s]$ channel is prolate, while the $[\bar{d}c][\bar{d}s]$ and both $D^*\bar{K}^*$ configurations are oblate. Although the dominant configuration of these molecular candidates is expected to be S wave, relativistic quark-gluon dynamics and spin-orbit correlations within the LCSR framework can be interpreted as arising from small D -wave or tensor admixtures, which in turn generate finite quadrupole moments. The resulting hierarchy,

$$|\mathcal{D}_{D^*\bar{K}}| > |\mathcal{D}_{D\bar{K}^*}| > |\mathcal{D}_{D^*\bar{K}^*}|,$$

suggests that such anisotropic components are most pronounced in the $D^*\bar{K}$ channel, likely reflecting a stronger interplay between the vector meson polarization and the spatial separation of the light-quark charges.

Overall, the modest magnitude of the quadrupole moments indicates that these states are only weakly deformed and spatially extended, which is qualitatively consistent with expectations for loosely bound molecular configurations, although a definitive discrimination from more compact multiquark scenarios would require additional observables.

3. Phenomenological consequences and accessible observables

Although the magnetic and quadrupole moments are static quantities, they encode information about the electromagnetic structure of the states and may affect processes involving real or virtual photons. Consequently, they can lead to potentially observable effects in production mechanisms, radiative transitions, and other electromagnetic probes.

States with comparatively large magnetic moments are expected to exhibit enhanced couplings to external electromagnetic fields and may therefore be more sensitive to photon-induced production channels. At the level of dimensional analysis, or within simple effective hadronic descriptions, the near-threshold photoproduction cross section for reactions such as $\gamma p \rightarrow T_{cs} + X$ can be parametrically estimated to scale schematically as

$$\sigma(\gamma p \rightarrow T_{cs} + X) \propto \frac{\alpha}{m_{T_{cs}}^2} \mu_{T_{cs}}^2,$$

which should be interpreted only as an order-of-magnitude estimate rather than a quantitative prediction. In practice, realistic cross sections depend on additional ingredients such as hadronic form factors, production dynamics, and final-state interactions, effects that lie beyond the scope of the present LCSR framework. Nevertheless, magnetic moments of order $\mu_{T_{cs}} \sim 2\text{--}3 \mu_N$, as obtained here, suggest that electromagnetic production mechanisms may be experimentally accessible. Similar qualitative sensitivities may also arise in initial-state radiation processes such as $e^+e^- \rightarrow T_{cs}\gamma$ or $pp \rightarrow T_{cs}\gamma + X$, where the magnetic moment can influence both the overall rate and the angular distributions of the emitted photon.

Electromagnetic moments also enter radiative transitions between possible partner states. If excited configurations exist, the widths of $T_{cs}^* \rightarrow T_{cs}\gamma$ decays are governed by magnetic dipole (M1) matrix elements closely related to the static moments and scale approximately as

$$\Gamma(T_{cs}^* \rightarrow T_{cs}\gamma) \sim \frac{\alpha}{3} \frac{k^3}{m_{T_{cs}}^2} |\mu_{T_{cs}}|^2,$$

where k denotes the photon momentum in the rest frame. The same magnetic form factor also controls Dalitz decays through $F_M(Q^2)$, providing additional indirect access to the electromagnetic structure. Furthermore, strong external electromagnetic fields generated in heavy-ion or polarized-hadron environments may induce spin-alignment effects for states with nonzero magnetic moments, offering complementary, though experimentally challenging, probes of their internal dynamics.

From the theoretical perspective, the present LCSR predictions provide useful benchmarks for comparison with alternative approaches such as lattice QCD calculations or effective field theories describing heavy-meson molecules. The observed dominance of light-quark contributions, the suppression of the charm-quark term, and the hierarchy $\mu_{D^*\bar{K}} > \mu_{D\bar{K}^*} \simeq \mu_{D^*\bar{K}^*}$ represent qualitative features that are compatible with a molecular scenario. Significant deviations from this pattern could instead indicate more compact configurations, for instance diquark-antidiquark tetraquarks or hadro-charmonium states. In this sense, electromagnetic moments may serve as informative quantitative discriminants of the internal structure.

We emphasize, however, that the present LCSR analysis does not provide a model-independent determination of the internal composition, nor does it attempt a direct comparison with compact tetraquark interpolators. The extracted electromagnetic moments should therefore be regarded as being consistent with, rather than proving, a loosely bound molecular interpretation. A decisive discrimination between different structural scenarios will ultimately require complementary theoretical calculations and dedicated experimental measurements.

IV. DISCUSSION AND OUTLOOK

In this work, we have investigated the electromagnetic properties of three charm–strange molecular configurations, $D\bar{K}^*$, $D^*\bar{K}$, and $D^*\bar{K}^*$, with quantum numbers $J^P = 1^+$. Using the framework of QCD light–cone sum rules, analytic expressions for the magnetic and quadrupole moments were obtained by matching the hadronic and operator–product–expansion representations of an appropriate correlation function. Both short–distance photon couplings and long–distance contributions encoded in photon distribution amplitudes were consistently taken into account. After fixing the auxiliary parameters according to standard sum–rule criteria, numerical results were extracted and summarized in Tables III and IV. The reliability of the sum–rule analysis is supported by standard consistency checks. In the selected Borel windows, pole contributions lie in the range of 40%–70%, and the convergence of the operator–product expansion is excellent. In particular, the relative contribution of the highest–dimensional (dimension–7) terms remains below 0.5% for all channels, demonstrating that the truncation of the OPE is well under control. The quoted uncertainties arise mainly from the variations of the continuum threshold, hadron masses and residues, the Borel parameter, and the nonperturbative input parameters.

An analysis of flavor contributions shows that the magnetic response is largely governed by the light quarks, while the charm–quark contribution is suppressed by the heavy–quark mass. This behavior is naturally compatible with the interpretation of these systems as loosely bound hadronic molecules, where the heavy quark acts predominantly as a static color source. The fully neutral $D\bar{K}^*$ configuration has vanishing electromagnetic moments due to overall charge neutrality, whereas the neutral $D^*\bar{K}$ and $D^*\bar{K}^*$ states acquire nonzero moments since they are not charge–conjugation eigenstates in the molecular picture.

To our knowledge, this work represents one of the first dedicated QCD light–cone sum rule studies of electromagnetic moments for $D^{(*)}\bar{K}^{(*)}$ molecular states. The results provide quantitative benchmarks that can be compared with future predictions from constituent quark models, effective field theories for heavy–meson molecules, or lattice QCD calculations. In particular, the hierarchy of magnetic moments and the small but nonzero quadrupole deformations may provide useful quantitative information that can help discriminate between molecular configurations and more compact multiquark interpretations.

From the perspective of the phenomenology of open-flavor charm–strange exotic states reported by LHCb, several candidates with quantum numbers $J^P = 0^+$ and 1^- are frequently discussed in the literature as possible $D^{(*)}\bar{K}^{(*)}$ hadronic molecules. Although the present analysis focuses on the $D^*\bar{K}^*$ configuration with $J^P = 1^+$, the electromagnetic properties obtained here may still provide qualitative insight into the internal structure of nearby molecular states in the same mass region.

In conclusion, electromagnetic moments provide valuable insight into the internal structure of exotic hadrons. The present analysis indicates that charm–strange molecular states exhibit characteristic magnetic and quadrupole moments that are compatible with an extended two–meson configuration. We expect that ongoing experimental efforts, together with further theoretical developments, will help clarify the nature of these states and deepen our understanding of multiquark dynamics.

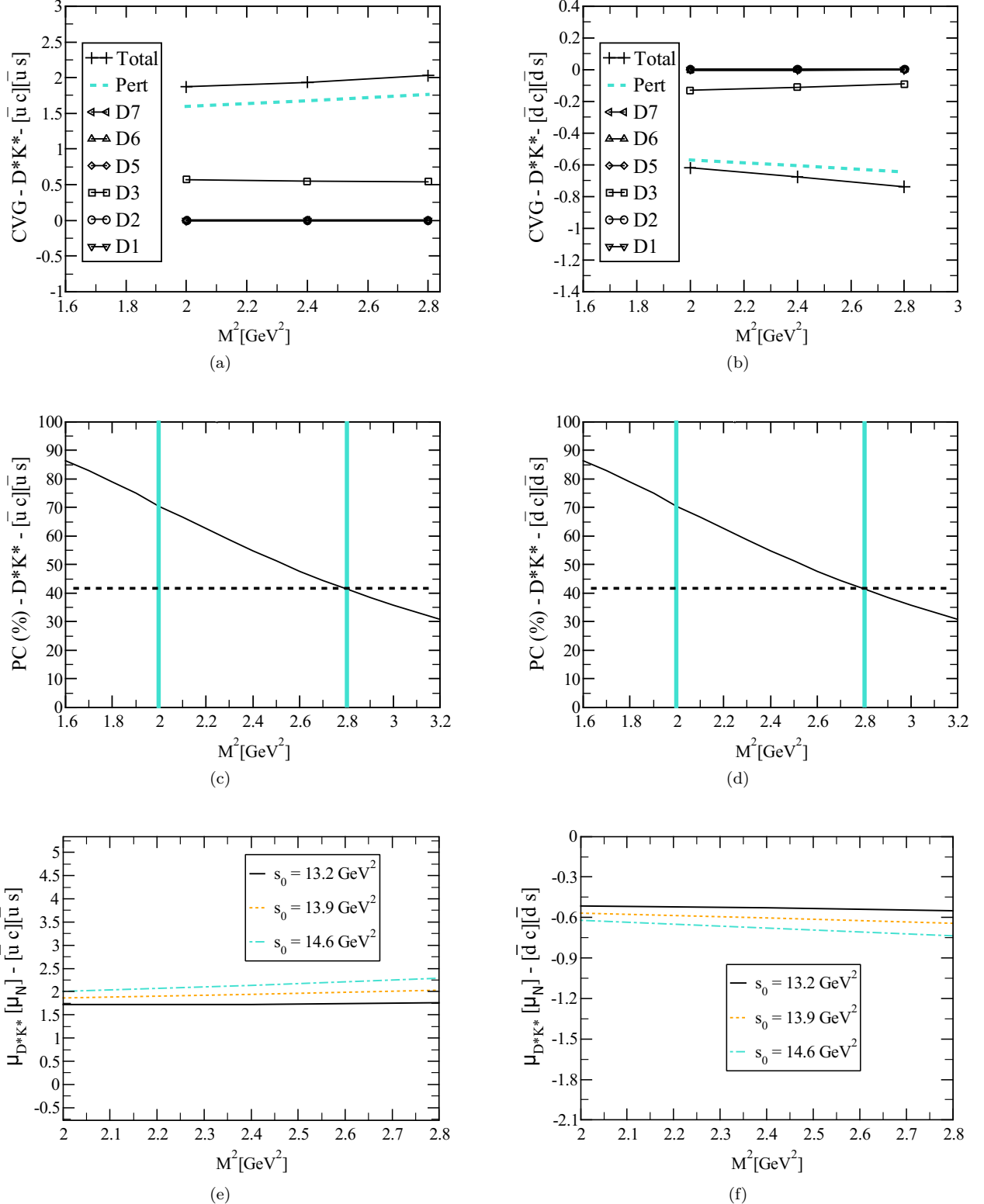


FIG. 1. Dependence of the sum-rule diagnostics and the extracted magnetic dipole moment on the Borel mass M^2 for the molecular $D^* K^*$ configuration. Panels (a) and (b) show the convergence of the CVG for the $[\bar{u}c]\bar{u}s$ and $[\bar{d}c]\bar{d}s$ flavor compositions, respectively. Panels (c) and (d) display the corresponding PC. In all four panels, the curves are obtained by varying the continuum threshold s_0 over the interval given in Table II. Panels (e) and (f) show the magnetic moment as a function of M^2 for several fixed representative values of s_0 . The vertical dashed lines mark the adopted Borel working window, and the horizontal dashed line in panels (c) and (d) indicates the minimum acceptable pole contribution (40%).

APPENDIX: SUM RULES FOR THE MAGNETIC DIPOLE MOMENTS

The resulting sum rules for the magnetic moments of the $D\bar{K}^*$, $D^*\bar{K}$, and $D^*\bar{K}^*$ molecular states can be written as

$$\begin{aligned} \mathcal{R}_1(M^2, s_0) = & -(e_s - e_q) \frac{m_c^2}{2048\pi^6} \left[7m_c^{10}I[-2] + 27m_c^6I[0] - 2m_c^4I[1] + 32I[3] \right] \\ & + \frac{\langle g_s^2 G^2 \rangle \langle \bar{q}q \rangle}{73728m_c\pi^4} (e_s - e_q) \left[-12m_c^2\mathbb{A}[u_0]I[0] + (13I_4[\mathcal{S}] + 12(-I_4[\tilde{\mathcal{S}}] + 2I_6[\varphi_\gamma]))(2m_c^2I[0] - I[1]) \right] \\ & + \frac{13\langle g_s^2 G^2 \rangle f_{3\gamma}}{147456m_c^2\pi^4} (e_s - e_q) \left[(2m_c^6I[-1] + m_c^4I[0] + I[2])I_1[\mathcal{V}] \right] \\ & + \frac{f_{3\gamma}}{2048\pi^4} (e_s - e_q) \left[(m_c^8I[-1] + m_c^6I[0] + 2I[3])I_1[\mathcal{V}] \right], \end{aligned} \quad (35)$$

$$\begin{aligned} \mathcal{R}_3(M^2, s_0) = & \frac{m_c^2}{8192\pi^6} \left[4e_q(7m_c^{10}I[-2] + 27m_c^6I[0] - 2m_c^4I[1] + 32I[3]) - e_c(m_c^{10}I[-2] + 32m_c^8I[-1] - 6m_c^6I[0] \right. \\ & \left. + 40m_c^4I[1] - 3m_c^2I[2] + 64I[3]) \right] \\ & + \frac{e_q \langle g_s^2 G^2 \rangle \langle \bar{q}q \rangle}{36864m_c\pi^4} \left[2m_c^2(6\mathbb{A}[u_0] + 13I_4[\mathcal{S}] + 12I_4[\tilde{\mathcal{S}}])I[0] - (13I_4[\mathcal{S}] + 12(I_4[\tilde{\mathcal{S}}] + 2I_6[h_\gamma]))I[1] \right] \\ & - \frac{e_q \langle g_s^2 G^2 \rangle f_{3\gamma}}{147456m_c^2\pi^4} \left[13(2m_c^6I[-1] + m_c^4I[0] + I[2])I_1[\mathcal{V}] + 24I_5[\psi^a](2m_c^8I[-2] + m_c^4I[0] - 4m_c^2I[1] + I[2]) \right. \\ & \left. + 48(2m_c^8I[-2] + 3m_c^4I[0] - 2m_c^2I[1] + I[2])\psi^a[u_0] \right] \\ & - \frac{e_q \langle g_s^2 G^2 \rangle \langle \bar{q}q \rangle \chi}{1536m_c\pi^4} \left[(2m_c^6I[-1] + m_c^4I[0] + I[2])\varphi_\gamma[u_0] \right] \\ & + \frac{3e_q m_c^3 \langle \bar{q}q \rangle}{512\pi^4} \left[-2m_c^6I_6[h_\gamma]I[-2] - m_c^4(2\mathbb{A}[u_0] + I_4[\mathcal{S}] + I_4[\tilde{\mathcal{S}}] + 4I_6[h_\gamma])I[-1] + 2m_c^2(\mathbb{A}[u_0] + I_4[\mathcal{S}] \right. \\ & \left. + I_4[\tilde{\mathcal{S}}] + I_6[h_\gamma])I[0] - (I_4[\mathcal{S}] + I_4[\tilde{\mathcal{S}}])I[1] \right] \\ & - \frac{e_q f_{3\gamma}}{1024\pi^4} \left[2(m_c^{10}I[-2] + 2m_c^8I[-1] + m_c^6I[0] + 4I[3])I_5[\psi^a] + (m_c^8I[-1] + 2m_c^6I[0] + m_c^4I[1] + 4I[3])I_1[\mathcal{V}] \right. \\ & \left. + 4m_c^6(m_c^4I[-2] - I[0])\psi^a[u_0] \right], \end{aligned} \quad (36)$$

$$\begin{aligned} \mathcal{R}_5(M^2, s_0) = & -\frac{m_c}{8192\pi^6} \left[12e_s \left(7m_c^{11}I[-2] + 27m_c^7I[0] - 2m_c^5I[1] + 32m_cI[3] \right) - 16e_q \left(7m_c^{11}I[-2] + 21m_c^{10}m_sI[-2] \right. \right. \\ & \left. + 27m_c^7I[0] + 45m_c^6m_sI[0] - 2m_c^5I[1] - 6m_c^4m_sI[1] + 32m_cI[3] + 60m_sI[3] \right) + e_c \left(3m_c^{11}I[-2] \right. \\ & \left. + 96m_c^9I[-1] + 32m_c^8m_sI[-1] - 18m_c^7I[0] + 96m_c^6m_sI[0] + 120m_c^5I[1] + 96m_c^4m_sI[1] - 9m_c^3I[2] \right. \\ & \left. + 32m_c^2m_sI[2] + 192m_cI[3] + 256m_sI[3] \right) \\ & + \frac{\langle g_s^2 G^2 \rangle \langle \bar{q}q \rangle}{36864m_c\pi^4} \left[3e_s m_c^2(8I_2[\mathcal{S}] + 11I_2[\tilde{\mathcal{S}}])I[0] + e_q(17I_4[\tilde{\mathcal{S}}] - 15I_4[\tilde{\mathcal{S}}])(-2m_c^2I[0] + I[1]) \right] \\ & - \frac{11\langle g_s^2 G^2 \rangle f_{3\gamma}}{147456m_c^2\pi^4} (e_s - 2e_q) \left[(2m_c^6I[-1] + m_c^4I[0] + I[2])I_1[\mathcal{V}] \right] \\ & - \frac{e_q m_c^3 \langle \bar{q}q \rangle}{512\pi^4} \left[3m_c^3((5m_c - 4m_s)I_4[\mathcal{S}] + m_c I_4[\tilde{\mathcal{S}}])I[-1] - 6m_c((3m_c - 2m_s)I_4[\mathcal{S}] + m_c I_4[\tilde{\mathcal{S}}])I[0] \right. \\ & \left. + 3m_c(m_c - m_s)I_1[\mathcal{S}](m_c^4I[-2] - 2m_c^2I[-1] + I[0]) + (m_c^5(5m_c + 3m_s)I[-2] - 6m_c^3(2m_c + m_s)I[-1] \right. \\ & \left. + 3m_c(3m_c + m_s)I[0] - 2I[1])I_1[\tilde{\mathcal{S}}] + 3(I_4[\mathcal{S}] + I_4[\tilde{\mathcal{S}}])I[1] \right] \\ & + \frac{e_s m_c^2 \langle \bar{s}s \rangle}{256\pi^4} \left[3m_c^7(I_1[\mathcal{S}] + I_1[\tilde{\mathcal{S}}] + 2(I_2[\mathcal{S}] + I_2[\tilde{\mathcal{S}}]))I[-2] - 6m_c^5(I_1[\mathcal{S}] + I_1[\tilde{\mathcal{S}}] + 2I_2[\tilde{\mathcal{S}}])I[-1] \right. \\ & \left. + (3m_c^3(I_1[\mathcal{S}] + I_1[\tilde{\mathcal{S}}] - 2I_2[\mathcal{S}] + 2I_2[\tilde{\mathcal{S}}]) + 32(I_2[\mathcal{S}] + 3I_2[\tilde{\mathcal{S}}]))I[0] \right] \end{aligned}$$

$$\begin{aligned}
& + \frac{f_{3\gamma}}{3072\pi^4} \left[(e_q m_c^3 (4m_c^7 I[-2] - 3m_c^5 I[-1] + 18m_c^4 m_s I[-1] - 36m_c^2 m_s I[0] + 7m_c I[1] + 18m_s I[1]) + 8e_q I[3] \right. \\
& \left. + 6e_s (-m_c^{10} I[-2] + m_c^8 I[-1] + 2m_c^6 I[0] + 2I[3])) I_1[\mathcal{V}] \right]. \tag{37}
\end{aligned}$$

Here, $\langle g_s^2 G^2 \rangle$ denotes the gluon condensate, while $\langle \bar{q}q \rangle$ and $\langle \bar{s}s \rangle$ represent the light (u, d) and strange quark condensates, respectively. The convolution integrals $I[n]$ and $I_i[\mathcal{A}]$ ($i = 1, \dots, 6$), which encode the spectral and distribution-amplitude contributions entering the sum rules, are defined as follows:

$$\begin{aligned}
I[n] &= \int_{\mathcal{M}}^{s_0} ds s^n e^{-s/M^2} \\
I_1[\mathcal{A}] &= \int D_{\alpha_i} \int_0^1 dv \mathcal{A}(\alpha_{\bar{q}}, \alpha_q, \alpha_g) \delta'(\alpha_q + \bar{v}\alpha_g - u_0), \\
I_2[\mathcal{A}] &= \int D_{\alpha_i} \int_0^1 dv \mathcal{A}(\alpha_{\bar{q}}, \alpha_q, \alpha_g) \delta'(\alpha_{\bar{q}} + v\alpha_g - u_0), \\
I_3[\mathcal{A}] &= \int_0^1 du A(u) \delta'(u - u_0), \\
I_4[\mathcal{A}] &= \int D_{\alpha_i} \int_0^1 dv \mathcal{A}(\alpha_{\bar{q}}, \alpha_q, \alpha_g) \delta(\alpha_q + \bar{v}\alpha_g - u_0), \\
I_5[\mathcal{A}] &= \int D_{\alpha_i} \int_0^1 dv \mathcal{A}(\alpha_{\bar{q}}, \alpha_q, \alpha_g) \delta(\alpha_{\bar{q}} + v\alpha_g - u_0), \\
I_6[\mathcal{A}] &= \int_0^1 du A(u).
\end{aligned}$$

Here, $\mathcal{M} = (m_c + m_s)^2$, \mathcal{A} represents the photon DAs, and the measure $D\alpha_i$ is given by

$$\int D\alpha_i = \int_0^1 d\alpha_{\bar{q}} \int_0^1 d\alpha_q \int_0^1 d\alpha_g \delta(1 - \alpha_{\bar{q}} - \alpha_q - \alpha_g). \tag{38}$$

-
- [1] S. K. Choi, et al., Observation of a narrow charmonium-like state in exclusive $B^\pm \rightarrow K^\pm \pi^+ \pi^- J/\psi$ decays, Phys. Rev. Lett. 91 (2003) 262001. [arXiv:hep-ex/0309032](https://arxiv.org/abs/hep-ex/0309032), doi:10.1103/PhysRevLett.91.262001.
- [2] A. Esposito, A. L. Guerrieri, F. Piccinini, A. Pilloni, A. D. Polosa, Four-Quark Hadrons: an Updated Review, Int. J. Mod. Phys. A 30 (2015) 1530002. [arXiv:1411.5997](https://arxiv.org/abs/1411.5997), doi:10.1142/S0217751X15300021.
- [3] A. Esposito, A. Pilloni, A. D. Polosa, Multiquark Resonances, Phys. Rept. 668 (2017) 1–97. [arXiv:1611.07920](https://arxiv.org/abs/1611.07920), doi:10.1016/j.physrep.2016.11.002.
- [4] S. L. Olsen, T. Skwarnicki, D. Zieminska, Nonstandard heavy mesons and baryons: Experimental evidence, Rev. Mod. Phys. 90 (1) (2018) 015003. [arXiv:1708.04012](https://arxiv.org/abs/1708.04012), doi:10.1103/RevModPhys.90.015003.
- [5] R. F. Lebed, R. E. Mitchell, E. S. Swanson, Heavy-Quark QCD Exotica, Prog. Part. Nucl. Phys. 93 (2017) 143–194. [arXiv:1610.04528](https://arxiv.org/abs/1610.04528), doi:10.1016/j.ppnp.2016.11.003.
- [6] M. Nielsen, F. S. Navarra, S. H. Lee, New Charmonium States in QCD Sum Rules: A Concise Review, Phys. Rept. 497 (2010) 41–83. [arXiv:0911.1958](https://arxiv.org/abs/0911.1958), doi:10.1016/j.physrep.2010.07.005.
- [7] N. Brambilla, S. Eidelman, C. Hanhart, A. Nefediev, C.-P. Shen, C. E. Thomas, A. Vairo, C.-Z. Yuan, The XYZ states: experimental and theoretical status and perspectives, Phys. Rept. 873 (2020) 1–154. [arXiv:1907.07583](https://arxiv.org/abs/1907.07583), doi:10.1016/j.physrep.2020.05.001.
- [8] S. Agaev, K. Azizi, H. Sundu, Four-quark exotic mesons, Turk. J. Phys. 44 (2) (2020) 95–173. [arXiv:2004.12079](https://arxiv.org/abs/2004.12079), doi:10.3906/fiz-2003-15.
- [9] H.-X. Chen, W. Chen, X. Liu, S.-L. Zhu, The hidden-charm pentaquark and tetraquark states, Phys. Rept. 639 (2016) 1–121. [arXiv:1601.02092](https://arxiv.org/abs/1601.02092), doi:10.1016/j.physrep.2016.05.004.
- [10] A. Ali, J. S. Lange, S. Stone, Exotics: Heavy Pentaquarks and Tetraquarks, Prog. Part. Nucl. Phys. 97 (2017) 123–198. [arXiv:1706.00610](https://arxiv.org/abs/1706.00610), doi:10.1016/j.ppnp.2017.08.003.
- [11] F.-K. Guo, C. Hanhart, U.-G. Meißner, Q. Wang, Q. Zhao, B.-S. Zou, Hadronic molecules, Rev. Mod. Phys. 90 (1) (2018) 015004, [Erratum: Rev. Mod. Phys. 94, 029901 (2022)]. [arXiv:1705.00141](https://arxiv.org/abs/1705.00141), doi:10.1103/RevModPhys.90.015004.
- [12] Y.-R. Liu, H.-X. Chen, W. Chen, X. Liu, S.-L. Zhu, Pentaquark and Tetraquark states, Prog. Part. Nucl. Phys. 107 (2019) 237–320. [arXiv:1903.11976](https://arxiv.org/abs/1903.11976), doi:10.1016/j.ppnp.2019.04.003.
- [13] G. Yang, J. Ping, J. Segovia, Tetra- and penta-quark structures in the constituent quark model, Symmetry 12 (11) (2020) 1869. [arXiv:2009.00238](https://arxiv.org/abs/2009.00238), doi:10.3390/sym12111869.

- [14] X.-K. Dong, F.-K. Guo, B.-S. Zou, A survey of heavy-antiheavy hadronic molecules, *Progr. Phys.* 41 (2021) 65–93. [arXiv:2101.01021](https://arxiv.org/abs/2101.01021), [doi:10.13725/j.cnki.pip.2021.02.001](https://doi.org/10.13725/j.cnki.pip.2021.02.001).
- [15] X.-K. Dong, F.-K. Guo, B.-S. Zou, A survey of heavy-heavy hadronic molecules, *Commun. Theor. Phys.* 73 (12) (2021) 125201. [arXiv:2108.02673](https://arxiv.org/abs/2108.02673), [doi:10.1088/1572-9494/ac27a2](https://doi.org/10.1088/1572-9494/ac27a2).
- [16] H.-X. Chen, W. Chen, X. Liu, Y.-R. Liu, S.-L. Zhu, An updated review of the new hadron states, *Rept. Prog. Phys.* 86 (2) (2023) 026201. [arXiv:2204.02649](https://arxiv.org/abs/2204.02649), [doi:10.1088/1361-6633/aca3b6](https://doi.org/10.1088/1361-6633/aca3b6).
- [17] L. Meng, B. Wang, G.-J. Wang, S.-L. Zhu, Chiral perturbation theory for heavy hadrons and chiral effective field theory for heavy hadronic molecules, *Phys. Rept.* 1019 (2023) 1–149. [arXiv:2204.08716](https://arxiv.org/abs/2204.08716), [doi:10.1016/j.physrep.2023.04.003](https://doi.org/10.1016/j.physrep.2023.04.003).
- [18] R. Aaij, et al., Amplitude analysis of the $B^+ \rightarrow D^+ D^- K^+$ decay, *Phys. Rev. D* 102 (2020) 112003. [arXiv:2009.00026](https://arxiv.org/abs/2009.00026), [doi:10.1103/PhysRevD.102.112003](https://doi.org/10.1103/PhysRevD.102.112003).
- [19] R. Aaij, et al., A model-independent study of resonant structure in $B^+ \rightarrow D^+ D^- K^+$ decays, *Phys. Rev. Lett.* 125 (2020) 242001. [arXiv:2009.00025](https://arxiv.org/abs/2009.00025), [doi:10.1103/PhysRevLett.125.242001](https://doi.org/10.1103/PhysRevLett.125.242001).
- [20] R. Aaij, et al., Amplitude analysis of $B0 \rightarrow D^- 0Ds + \pi^-$ and $B+ \rightarrow D-Ds + \pi^+$ decays, *Phys. Rev. D* 108 (1) (2023) 012017. [arXiv:2212.02717](https://arxiv.org/abs/2212.02717), [doi:10.1103/PhysRevD.108.012017](https://doi.org/10.1103/PhysRevD.108.012017).
- [21] R. Aaij, et al., First Observation of a Doubly Charged Tetraquark and Its Neutral Partner, *Phys. Rev. Lett.* 131 (4) (2023) 041902. [arXiv:2212.02716](https://arxiv.org/abs/2212.02716), [doi:10.1103/PhysRevLett.131.041902](https://doi.org/10.1103/PhysRevLett.131.041902).
- [22] R. Aaij, et al., Observation of New Charmonium or Charmoniumlike States in $B+ \rightarrow D^* \pm D \mp K \mp$ Decays, *Phys. Rev. Lett.* 133 (13) (2024) 131902. [arXiv:2406.03156](https://arxiv.org/abs/2406.03156), [doi:10.1103/PhysRevLett.133.131902](https://doi.org/10.1103/PhysRevLett.133.131902).
- [23] R. Molina, E. Oset, Molecular picture for the $X_0(2866)$ as a $D^* \bar{K}^* J^P = 0^+$ state and related $1^+, 2^+$ states, *Phys. Lett. B* 811 (2020) 135870, [Erratum: *Phys.Lett.B* 837, 137645 (2023)]. [arXiv:2008.11171](https://arxiv.org/abs/2008.11171), [doi:10.1016/j.physletb.2020.135870](https://doi.org/10.1016/j.physletb.2020.135870).
- [24] L. R. Dai, R. Molina, E. Oset, The $B^- 0 \rightarrow D^* + D^- * 0 K^-$ reaction to detect the $I = 0, J^P = 1^+$ partner of the $X_0(2866)$, *Phys. Lett. B* 832 (2022) 137219. [arXiv:2202.00508](https://arxiv.org/abs/2202.00508), [doi:10.1016/j.physletb.2022.137219](https://doi.org/10.1016/j.physletb.2022.137219).
- [25] H. Sundu, S. S. Agaev, K. Azizi, Axial-vector and pseudoscalar tetraquarks $[ud][\bar{c}\bar{s}]$, *Eur. Phys. J. C* 83 (3) (2023) 198. [arXiv:2206.05004](https://arxiv.org/abs/2206.05004), [doi:10.1140/epjc/s10052-023-11339-8](https://doi.org/10.1140/epjc/s10052-023-11339-8).
- [26] K. Azizi, U. Özdem, Magnetic dipole moments of the Tcc+ and ZV++ tetraquark states, *Phys. Rev. D* 104 (11) (2021) 114002. [arXiv:2109.02390](https://arxiv.org/abs/2109.02390), [doi:10.1103/PhysRevD.104.114002](https://doi.org/10.1103/PhysRevD.104.114002).
- [27] S. S. Agaev, K. Azizi, H. Sundu, Doubly charged vector tetraquark $Z_V^{++} = [cu][\bar{s}\bar{d}]$, *Phys. Lett. B* 820 (2021) 136530. [arXiv:2105.00081](https://arxiv.org/abs/2105.00081), [doi:10.1016/j.physletb.2021.136530](https://doi.org/10.1016/j.physletb.2021.136530).
- [28] V. L. Chernyak, I. R. Zhitnitsky, B meson exclusive decays into baryons, *Nucl. Phys. B* 345 (1990) 137–172. [doi:10.1016/0550-3213\(90\)90612-H](https://doi.org/10.1016/0550-3213(90)90612-H).
- [29] V. M. Braun, I. E. Filyanov, QCD Sum Rules in Exclusive Kinematics and Pion Wave Function, *Z. Phys. C* 44 (1989) 157. [doi:10.1007/BF01548594](https://doi.org/10.1007/BF01548594).
- [30] I. I. Balitsky, V. M. Braun, A. V. Kolesnichenko, Radiative Decay $\Sigma^+ \rightarrow p \gamma$ in Quantum Chromodynamics, *Nucl. Phys. B* 312 (1989) 509–550. [doi:10.1016/0550-3213\(89\)90570-1](https://doi.org/10.1016/0550-3213(89)90570-1).
- [31] U. Özdem, Analysis of the $\Xi_c^* \bar{K}$ molecular pentaquark state by its electromagnetic properties, *Eur. Phys. J. C* 84 (7) (2024) 765. [arXiv:2407.08635](https://arxiv.org/abs/2407.08635), [doi:10.1140/epjc/s10052-024-13134-5](https://doi.org/10.1140/epjc/s10052-024-13134-5).
- [32] U. Özdem, Electromagnetic properties of Ω_c^0 resonances via light-cone QCD, *Eur. Phys. J. Plus* 139 (11) (2024) 978. [arXiv:2402.18901](https://arxiv.org/abs/2402.18901), [doi:10.1140/epjp/s13360-024-05779-8](https://doi.org/10.1140/epjp/s13360-024-05779-8).
- [33] U. Özdem, Analysis of the X_{AV} state through its electromagnetic properties, *Eur. Phys. J. C* 84 (4) (2024) 359. [arXiv:2401.00481](https://arxiv.org/abs/2401.00481), [doi:10.1140/epjc/s10052-024-12724-7](https://doi.org/10.1140/epjc/s10052-024-12724-7).
- [34] U. Özdem, Magnetic dipole moments of the $\Omega_c(3185)0$ and $\Omega_c(3327)0$ states from molecular perspective, *Phys. Lett. B* 849 (2024) 138432. [arXiv:2311.02925](https://arxiv.org/abs/2311.02925), [doi:10.1016/j.physletb.2023.138432](https://doi.org/10.1016/j.physletb.2023.138432).
- [35] U. Özdem, Electromagnetic properties of the $\Sigma_c(2800)^+$ and $\Lambda_c(2940)^+$ states via light-cone QCD, *Eur. Phys. J. C* 83 (11) (2023) 1077. [arXiv:2309.00959](https://arxiv.org/abs/2309.00959), [doi:10.1140/epjc/s10052-023-12251-x](https://doi.org/10.1140/epjc/s10052-023-12251-x).
- [36] U. Özdem, K. Azizi, Magnetic moment of the $X_1(2900)$ state in the diquark-antidiquark picture, *Eur. Phys. J. A* 58 (9) (2022) 171. [arXiv:2202.11466](https://arxiv.org/abs/2202.11466), [doi:10.1140/epja/s10050-022-00815-6](https://doi.org/10.1140/epja/s10050-022-00815-6).
- [37] U. Özdem, Magnetic moment of the $\Xi_b(6227)$ as a molecular pentaquark state, *Eur. Phys. J. Plus* 137 (1) (2022) 103. [arXiv:2109.09313](https://arxiv.org/abs/2109.09313), [doi:10.1140/epjp/s13360-022-02339-w](https://doi.org/10.1140/epjp/s13360-022-02339-w).
- [38] K. Azizi, U. Özdem, The electromagnetic multipole moments of the possible charm-strange pentaquarks in light-cone QCD, *Eur. Phys. J. C* 78 (9) (2018) 698. [arXiv:1807.06503](https://arxiv.org/abs/1807.06503), [doi:10.1140/epjc/s10052-018-6187-0](https://doi.org/10.1140/epjc/s10052-018-6187-0).
- [39] K. Azizi, U. Özdem, The electromagnetic multipole moments of the charged open-flavor $Z_{\bar{c}q}$ states, *J. Phys. G* 45 (5) (2018) 055003. [arXiv:1802.07711](https://arxiv.org/abs/1802.07711), [doi:10.1088/1361-6471/aab56b](https://doi.org/10.1088/1361-6471/aab56b).
- [40] U. Özdem, Electromagnetic properties of the $Ds1+(2460)$, $Ds1+(2536)$, and their bottom partners in a molecular configuration, *Phys. Rev. D* 112 (11) (2025) 114013. [arXiv:2510.17477](https://arxiv.org/abs/2510.17477), [doi:10.1103/y77p-ch1k](https://doi.org/10.1103/y77p-ch1k).
- [41] P. Ball, V. M. Braun, N. Kivel, Photon distribution amplitudes in QCD, *Nucl. Phys. B* 649 (2003) 263–296. [arXiv:hep-ph/0207307](https://arxiv.org/abs/hep-ph/0207307), [doi:10.1016/S0550-3213\(02\)01017-9](https://doi.org/10.1016/S0550-3213(02)01017-9).
- [42] V. A. Novikov, M. A. Shifman, A. I. Vainshtein, V. I. Zakharov, Calculations in External Fields in Quantum Chromodynamics. Technical Review, *Fortsch. Phys.* 32 (1984) 585.
- [43] B. L. Ioffe, A. V. Smilga, Nucleon Magnetic Moments and Magnetic Properties of Vacuum in QCD, *Nucl. Phys. B* 232 (1984) 109–142. [doi:10.1016/0550-3213\(84\)90364-X](https://arxiv.org/abs/10.1016/0550-3213(84)90364-X).
- [44] H.-X. Chen, Hadronic molecules in B decays, *Phys. Rev. D* 105 (9) (2022) 094003. [arXiv:2103.08586](https://arxiv.org/abs/2103.08586), [doi:10.1103/PhysRevD.105.094003](https://doi.org/10.1103/PhysRevD.105.094003).
- [45] I. I. Balitsky, V. M. Braun, Evolution Equations for QCD String Operators, *Nucl. Phys. B* 311 (1989) 541–584. [arXiv:hep-ph/9003001](https://arxiv.org/abs/hep-ph/9003001), [doi:10.1016/0550-3213\(89\)90030-1](https://doi.org/10.1016/0550-3213(89)90030-1).

- 10.1016/0550-3213(89)90168-5.
- [46] V. M. Belyaev, B. Y. Blok, CHARMED BARYONS IN QUANTUM CHROMODYNAMICS, *Z. Phys. C* 30 (1986) 151. [doi:10.1007/BF01560689](https://doi.org/10.1007/BF01560689).
- [47] D. Antonov, J. E. F. T. Ribeiro, Quark condensate for various heavy flavors, *Eur. Phys. J. C* 72 (2012) 2179. [arXiv:1209.0408](https://arxiv.org/abs/1209.0408), [doi:10.1140/epjc/s10052-012-2179-7](https://doi.org/10.1140/epjc/s10052-012-2179-7).
- [48] S. J. Brodsky, J. R. Hiller, Universal properties of the electromagnetic interactions of spin one systems, *Phys. Rev. D* 46 (1992) 2141–2149. [doi:10.1103/PhysRevD.46.2141](https://doi.org/10.1103/PhysRevD.46.2141).
- [49] S. Navas, et al., Review of particle physics, *Phys. Rev. D* 110 (3) (2024) 030001. [doi:10.1103/PhysRevD.110.030001](https://doi.org/10.1103/PhysRevD.110.030001).
- [50] B. L. Ioffe, QCD at low energies, *Prog. Part. Nucl. Phys.* 56 (2006) 232–277. [arXiv:hep-ph/0502148](https://arxiv.org/abs/hep-ph/0502148), [doi:10.1016/j.ppnp.2005.05.001](https://doi.org/10.1016/j.ppnp.2005.05.001).
- [51] S. Narison, $\bar{m}_{c,b} < \alpha_s G^2 >$ and α_s from Heavy Quarkonia, *Nucl. Part. Phys. Proc.* 300-302 (2018) 153–164. [doi:10.1016/j.nuclphysbps.2018.12.026](https://doi.org/10.1016/j.nuclphysbps.2018.12.026).
- [52] J. Rohrwild, Determination of the magnetic susceptibility of the quark condensate using radiative heavy meson decays, *JHEP* 09 (2007) 073. [arXiv:0708.1405](https://arxiv.org/abs/0708.1405), [doi:10.1088/1126-6708/2007/09/073](https://doi.org/10.1088/1126-6708/2007/09/073).